Arctic cloud cover bias in ECHAM6 and its sensitivity to cloud microphysics and surface fluxes

Jan Kretzschmar[1], Marc Salzmann[1], Johannes Mülmenstädt[1], and Johannes Quaas[1]

[1]Institute for Meteorology, Universität Leipzig, Vor dem Hospitaltore 1, 04103 Leipzig, Germany

Correspondence: Jan Kretzschmar (jan.kretzschmar@uni-leipzig.de)

Abstract. Among the many different feedback mechanisms contributing to the Arctic Amplification, clouds play a very important role in the Arctic climate system through their cloud radiative effect. It is therefore important that climate models simulate basic cloud properties like cloud cover and cloud phase correctly. We compare results from the global atmospheric model ECHAM6 to observations from the CALIPSO satellite active lidar instrument using the COSP satellite simulator. Our results

5   show that the model is able to reproduce the spatial distribution and cloud amount in the Arctic to some extent, but that cloud cover has a positive bias (caused by an overestimation of low-level, liquid containing cloud) in regions where the surface is covered by snow or ice. We explored the sensitivity of cloud cover to the strength of surface heat fluxes, but only by increasing surface mixing the observed cloud cover bias cloud be reduced. As ECHAM6 already mixes too strongly in the Arctic, the cloud cover bias can mainly be attributed to cloud microphysical processes. Improvements in the phase partitioning of Arctic

10   low-level clouds could be achieved by a more effective Wegener-Bergeron-Findeisen process but total cloud cover remained still overestimated. By allowing for a slight supersaturation with respect to ice within the cloud cover scheme, we were able to also reduce this positive cloud cover bias.

Copyright statement. TEXT

1 Introduction

15   With temperatures rising nearly twice as strongly compared to the temperature increase of the Northern Hemisphere (Screen and Simmonds, 2010), the Arctic reacts especially susceptibly to global climate change. This is due to several positive feedback mechanisms that strengthen the warming in the high latitudes (Serreze and Barry, 2011). This so called Arctic Amplification has important implications on the Arctic climate system like the extreme decrease in summer sea ice extent in recent years, the thawing of permafrost or the melting of glaciers in Greenland. Besides those effects on the regional scale, it is believed that the

20   Arctic Amplification might have effects on the atmospheric circulation due to a decrease in the temperature gradient between mid and high latitudes (Francis and Vavrus, 2012). Additionally, the melting glaciers in Greenland contribute to the sea level rise, which will affect many coastal areas around the globe.

While globally having a cooling effect, clouds in the Arctic warm the surface most of the year except a short period in summer

(Intrieri, 2002; Zygmuntowska et al., 2012; Kay and L'Ecuyer, 2013). As the amount of clouds is thought to increase in a warming Arctic (Liu et al., 2012), their positive cloud radiative effect (CRE) can further enhance Arctic Amplification. Using global climate models (GCMs) to assess the CRE in the Arctic on a larger scale is inevitable because of the complexity of the climate system in the Arctic. Due to this complexity, even present day estimations of the CRE from climate models in the Arctic are inconclusive (Karlsson and Svensson, 2013), as those models still struggle to correctly simulate even basic properties like cloud cover and cloud distribution (English et al., 2015; Boeke and Taylor, 2016), which complicates an assessment of future Arctic warming.

To improve the representation of clouds in climate models, it is important to compare their results to observations. Ground-based observations are usually fixed to a certain location and provide information on scales much smaller than those of GCMs. The difference in scales complicates the comparison of ground-based observations to simulations of climate models as those models cannot capture the small-scale heterogeneities present in observations. Another disadvantage of ground-based observations is that only a few sites in the Arctic conduct regular measurements of meteorological parameters, which also complicates a proper model evaluation. Nevertheless, those measurements provide valuable information on the climate in the Arctic and help to improve our understanding of many important processes in the Arctic climate system. An important tool often used in model evaluation is satellite remote sensing. Satellites can provide observations on spatial scales much closer to the scales of GCMs and are therefore well suited for assessing the performance of GCMs. Satellite remote sensing in the Arctic has to deal with several aspects that complicate their use in evaluating cloud properties in GCMs, which is especially the case for passive sensors. The polar night and often prevailing low-level inversions at high latitudes make it hard for passive instruments to discriminate between snow/sea ice and low-level clouds as they solely rely on the reflected and emitted radiation in the visible and thermal spectral ranges, respectively (Liu et al., 2010; Karlsson and Dybbroe, 2010). Active satellites like CloudSat (Stephens et al., 2002) and CALIPSO (Winker et al., 2003) are better suited, as they are less affected by the environmental conditions in the Arctic than passive sensors (Kay and L'Ecuyer, 2013; Zygmuntowska et al., 2012). With their active radar and lidar, they have largely improved our understanding of clouds and aerosols in the climate system. To facilitate the comparison of properties derived by satellites and the output from GCMs, the Cloud Feedback Model Intercomparison Project's (CFMIP) Observation Simulator Package (COSP; Bodas-Salcedo et al., 2011) has been developed. With the help of this satellite simulator, it is possible to consistently evaluate the results from GCMs by using common definitions of clouds observed from satellite and clouds simulated in GCMs. COSP has been used in various model evaluation studies (Nam and Quaas, 2012; Cesana and Chepfer, 2013; Nam et al., 2014), with some studies especially focusing on clouds in the Arctic (Barton et al., 2012; English et al., 2014; Kay et al., 2016). They show that some models have problems to correctly simulate the distribution and amount of clouds in the Arctic and also have problems to correctly simulate the phase state of clouds in high latitudes.

In the following, we will evaluate the performance of the atmospheric model ECHAM6 (Stevens et al., 2013) in the Arctic and will especially focus on the representation of clouds in this remote region. COSP is run online during the model integration. We will compare its output to CALIPSO datasets processed by the CFMIP Observations for Model Evaluation Project (CFMIP-OBS; Webb et al., 2017). Using these datasets ensures a consistent model-to-observation comparison as their diagnostics of observational data are consistent with the diagnostics within COSP.

2 Data and Model

2.1 CALIPSO

CALIPSO was launched in April 2006 and is part of the A-Train. This constellation of satellites is flying in a polar, sun-synchronous orbit. Their orbit has an inclination of 98.2°and the satellites cross the ascending/descending node at 1330/0130
local solar time. Due to their inclination and due to the fact that only a narrow swath at nadir is observed, the satellites can only retrieve information from 82°N to 82°S. It takes 16 days for the satellite to sample again the same swath. The fact that there is no information available north of 82°N is disadvantageous for our study, but in return, all regions close to the northern boundary of 82°N are sampled with a high temporal frequency due to the inclination of the orbit.

The Cloud-Aerosol Lidar and Infrared Pathfinder Satellite Observations satellite (CALIPSO Winker et al., 2003) hosts a lidar that provides high resolution profiles of clouds and aerosols. This lidar - the Cloud-Aerosol Lidar with Orthogonal Polarization (CALIOP) - is a two wavelength (1064 nm, 532 nm), near-nadir looking lidar. Both channels are used to measure the lidar backscattering intensity. Comparing the backscattered intensity to that of a molecular atmosphere (no clouds or aerosols) gives the lidar scattering ratio. To further retrieve information on the properties of the particles (size, shape, type) that scatter the emitted light back to the sensor, CALIPSO has two receivers for the backscattered light at 532 nm that measure the two orthogonally polarized components of the backscattered lidar signal. We use CALIPSO data from the GCM-Oriented CALIPSO Cloud Product (GOCCP) dataset (Chepfer et al., 2010), which is generated from CALIOP Level 1B NASA Langley Atmospheric Sciences Data Center CALIPSO datasets. The gridded data from CALIPSO-GOCCP (hereafter referred to as CALIPSO data) is available on a $2° \times 2°$grid and is consistent with the data generated by CALIPSO simulator within COSP as it uses the same cloud detection thresholds. In this study, we will evaluate cloud cover derived from CALIPSO in different altitudes bands (low, mid, high clouds), which are defined as follows:

$$
\begin{array}{lccl}
\text{high clouds} & & p_{top} & < 440\,\text{hPa} \\
\text{mid clouds} & 680\,\text{hPa} > & p_{top} & \geq 440\,\text{hPa} \\
\text{low clouds} & & p_{top} & \geq 680\,\text{hPa}
\end{array}
$$

The GOCCP product defines a cloud detection for scattering ratios larger than 5. Due to the ability of the satellite to retrieve information on the polarization of the signal, it is further possible to discriminate the phase state of the clouds seen by the lidar.

2.2 ECHAM6 and COSP

In this study, we use the atmospheric model ECHAM6 (Stevens et al., 2013) developed by the MPI in Hamburg. In all our simulation, the model is run at a resolution of T63, which is equivalent to a Gaussian grid of approximately $1.875° \times 1.875°$. In the vertical, we use a resolution of 47 levels. The model's vorticity and divergence are nudged to ERA-Interim reanalysis data (Dee et al., 2011) to enable comparison to satellite observations despite the relatively short run time of the model of less than 5 years. We use monthly observations of sea surface temperature and sea ice concentration as boundary conditions to further constrain the model.

To better compare the model results to the satellite observations, we use the Cloud Feedback Model Intercomparison Project's Observation Simulator Package (COSP; Bodas-Salcedo et al., 2011), version 1.4. Multiple satellite simulators are available within COSP, but here, only the simulator for CALIPSO (ActSim; Chepfer et al., 2008) is used. COSP uses model output like the profiles of temperature, pressure, cloud fraction, cloud water content, cloud particle concentration, as well as precipitation

10 flux of rain and snow from large-scale/convective precipitation as an input for its calculations. To account for subgrid scale variability of the cloud cover, COSP divides each model grid box into a specified number of subcolumns (here we use 40 subcolumns) that have a hydrometeor (cloud) fraction of either 1 or 0, so that the average over all subcolumns is equal to the hydrometeor (cloud) fraction of the model grid box. The calculations of the satellite simulators within COSP are then performed on each subcolumn to simulate specific signals received by instrument and to mimic the retrievals derived from

15 these instruments. By using the same instruments sensitivities and cloud overlap assumptions as used in the CFMIP-OBS dataset, COSP generates an output that is similar to the observations from satellites and also provides a common basis for comparing results from different climate models. The satellite simulator is implemented into ECHAM6 and is run online during the integration of the model. The output fields of COSP are interpolated on the $2° \times 2°$CFMIP-OBS grid for better comparison. For the evaluation of ECHAM6 in section 3, we run the model from 2007 to 2010, while for the sensitivity studies

20 in section 4 we only run it for 2007 and 2008 to reduce computational cost.

3 Arctic clouds and profiles of temperature and humidity in ECHAM6

In the following, we evaluate the temporal mean of a nudged ECHAM6 run for the years spanning 2007 to 2011 with prescribed sea surface temperatures and sea ice concentration and a spin-up of 6 months. The top row of Figure 1 shows the multi-year average distribution and amount of the total cloud cover for CALIPSO and ECHAM6 + COSP output. The bottom row shows

25 the difference from the CALIPSO observations. The black contour line indicates the extent of the snow/sea ice cover. An area is classified as covered with snow and ice if the average snow depth in the grid box is thicker than 2 cm or the sea ice fraction within a gridbox is greater than 50 %. ECHAM6 + COSP is able to reproduce the general cloud amount and distribution as observed by CALIPSO to some extent, but is biased high over the Arctic Ocean, Siberia and over the northern parts of Canada. Those areas correspond to areas that are covered with snow and sea ice, respectively.

30 To explore what causes the positive bias in cloud amount over snow and sea ice covered areas, it is important to know at which altitude the clouds are situated and of which thermodynamic phase (liquid or ice) they are composed. Figure 2 shows the meridional mean difference of ECHAM6 + COSP and CALISPO from 60°N to 82°N. Besides the difference in total cloud cover, Figure 2 also shows the difference in low, mid and high cloud cover (altitude bins defined as in subsection 2.1) as well as the difference in total liquid and total ice cloud cover. As low clouds are the most common cloud type in high latitudes, the difference in total cloud cover is strongly influenced by the difference of low-level clouds. For those low-level clouds, a clear influence of season and longitude on the difference in cloud cover can be observed, which is especially the case in winter and spring. During these two seasons and over nearly all regions (except the Atlantic Ocean), ECHAM6 + COSP simulates a

5 higher cloud cover than observed by CALIPSO. As seen in Figure 1, there seems to be a connection between the snow/sea ice

coverage of the surface which can also be observed in Figure 2. In contrast to low-level clouds, high-level clouds show no real dependency on longitude and only a weak dependency on the season and their amount is generally overestimated. For mid-level clouds, cloud cover almost perfectly matches the observations in spring and fall. whereas in summer, cloud cover is underestimated by the model. For all three seasons, no significant dependency on longitude is distinguishable. This is different

10   for winter, where the longitudinal behavior of the cloud cover bias is similar to that of low-level clouds. A possible explanation for this bias in mid-level clouds is that clouds that are considered to be low-level clouds in all other season are partly being accounted for as mid-level clouds due to the fact that the geopotential height of the 680 hPa pressure surface is lower during winter because of the colder temperatures of the atmosphere. When further discriminating between ice- and liquid-containing clouds (bottom row in Figure 2), one finds that this seasonal variation with a too large cloud cover in winter and spring mainly

15   stems from an overestimation of liquid-containing clouds that usually can be found in the lower troposphere. In the Arctic, liquid containing clouds are of special importance as those clouds strongly influence the radiative budget at the surface due to their large optical thickness and strong effect on net surface longwave radiation (Shupe and Intrieri, 2004) which causes a warming at the surface. For ice clouds, on the other hand, only very little seasonal or longitudinal variability in the deviation is distinguishable, and it is comparable to the difference in high cloud cover as those high clouds mainly consist of ice particles.

20   Taken together, ECHAM6 simulates low-level, liquid containing clouds too frequently, and this overestimation is connected to properties of the underlying surface.

To investigate what might be a cause for the overestimation of low-level, liquid-containing clouds in ECHAM6, we next assess how well the model is able to reproduce profiles of temperature and humidity in the Arctic. We therefore compare profiles of temperature and humidity from the model to profiles measured by radiosondes within high latitudes. To make the profiles of

25   the various stations independent of surface elevation, we use height above the ground as the vertical coordinate in our analysis and linearly interpolate the radiosonde data to altitudes above the surface spanning from 0 m to 3000 m in steps of 500 m. Using such a vertical coordinate facilitates the comparison of several stations that might vary in surface elevation. Additionally, it is independent of synoptic situation which would not be the case if one uses pressure as the vertical coordinate. A disadvantage of this vertical coordinate is that the surface elevation in the model is a grid-box mean which can deviate from the actual surface

30   elevation of the station but as most stations are situated near the coast or within the rather flat plains of the Siberian tundra, we expect only minor inconsistencies. One also has to keep in mind that the vertical resolution of the soundings and ECHAM6 is rather poor, so only a certain level of detail can be expected from them. Nevertheless, they provide a useful estimate of the vertical stratification of the atmosphere. Figure 3 shows that the model overestimates temperatures below 1000 m above ground level, while it simulates lower temperatures than measured by the radiosondes above this level. Especially at the surface,

35   temperatures in ECHAM6 are more than 1 K higher than observed. This positive temperature bias close to the surface might be related to the overestimation of low-level clouds as they exert a warming effect on the surface. The overestimated cloud cover can also be seen in the difference of absolute humidity as it is always higher than observed by the radiosondes. As the absolute humidity is limited by saturation humidity, and therefore decreases with decreasing temperature will also cause the differences to become smaller, so we also add the difference in relative humidity as it is temperature-independent. To ensure

5   comparability, relative humidity from the observations and the model is always calculated with respect to saturation pressure

over water. This is necessary as relative humidity in the model output can either be calculated with respect to water or with respect to ice, depending on the atmospheric condition (for more information. see section 4). As for the difference of absolute humidity, the difference in relative humidity between the model and the soundings is larger close to the surface (∼20 %) but decreases quite rapidly and is more or less constant at 7% above 1000 m and remains positive throughout the lower troposphere.

10 In general, the moisture content of the atmosphere can either be influenced by advection or local fluxes of moisture out of and into the atmosphere. As the positive bias in humidity is connected to snow and ice coverage of the surface, it is plausible that local effects are the cause for the observed bias. The cloud cover and moisture bias therefore implies that either the removal of atmospheric moisture by precipitation or fluxes of moisture from the surface into the atmosphere are not represented correctly in the model and that this seems to be connected to the underlying surface. Moisture fluxes into the atmosphere are directly

15 influenced by surface properties like surface roughness (which can be reduced by snow on the surface) or availability of humidity at the surface (which itself is a function of temperature) and indirectly through increased stability of the layers close to the surface that consequently has an influence on vertical mixing of momentum and latent/sensible heat fluxes. The linkage between surface properties and moisture removal can be established through the modification of the atmospheric stratification that consequently influences cloud microphysical processes. Over snow and ice covered surfaces, the strong radiative cooling

20 causes the temperatures to be significantly lower compared to a snow- and ice-free surface which may cause temperature-dependent processes like the Wegener-Bergeron-Findeisen (WBF) process or the heterogeneous freezing of cloud liquid water into ice to be more effective. As most precipitation in higher latitudes is formed via the ice phase, a higher ice content can lead to the dissipation of clouds, as can be seen in the rather rapid transition from the cloudy into the clear state that is often observed in the Arctic (Morrison et al., 2011).

25 4 Sensitivity studies

In this section, we will examine how sensitively cloud cover reacts to modified surface heat fluxes and to modifications of cloud microphysical parametrization. As the cloud bias is related to snow and ice covered surfaces, it is possible that fluxes of moisture from the surface into the atmosphere are not represented correctly in the model. In ECHAM6, turbulent surface fluxes of either heat ($\psi = h$) or momentum ($\psi = m$) are described using the following bulk-exchange formula:

30 $$\overline{w'\psi'} = -C_\psi\,|\boldsymbol{V}|\,(\psi_{\text{nlev}} - \psi_{\text{sfc}}),\tag{1}$$

where C_ψ is the bulk exchange coefficient with respect to ψ, $|\boldsymbol{V}|$ is the difference of the absolute wind velocity at the surface and the wind velocity in the lowest model level and the last term in parentheses is the difference of the respective quantity between the first model level (ψ_{nlev}) and at the surface (ψ_{sfc}). C_ψ can be further separated into the product of a neutral limit transfer coefficient $C_{\text{N},\psi}$ (which only depends on surface properties like surface roughness and the height of the first model level) and a (surface-layer) stability function f_ψ:

$$C_\psi = C_{\text{N},\psi}\,f_\psi\tag{2}$$

5   Those stability functions can be derived from Monin-Obukhov similarity theory by integrating the flux-profile relationships from the surface up to the lowest model layer but this is not practical for climate models. Therefore, ECHAM6 uses empirical expressions for those stability functions similar to the ones proposed by Louis (1979), depending on both surface properties and stability of the layer between the surface and the lowest model level (expressed by the moist Richardson number). To obtain a first impression on how cloud cover reacts to increased/decreased surface fluxes, we introduced a scaling factor μ into

10   Equation 2 so that it becomes:

$$C_\psi = \mu \, C_{\mathrm{N},\psi} \, f_\psi. \tag{3}$$

This scaling factor can be used to increase or decrease the neutral limit transfer coefficient which can be interpreted as a modification of the surface roughness, where values of μ greater than 1 denote higher surface roughness and stronger mixing, while values of μ less than 1 denote lower surface roughness and reduced mixing, respectively. We only modify this scaling

15   factor for snow and sea ice covered surfaces and set it to 1 elsewhere. As before, a surface is considered snow-covered when snow height is higher than an arbitrarily chosen value of 2 cm and, a surface is considered sea ice covered if more than 50 % a grid box is covered by sea ice. In Figure 4 we show the effect of increasing ($\mu = 5$) and decreasing ($\mu = 0.2$) mixing on low cloud cover over those surfaces in the northern hemisphere (for comparison we also added CALIPSO cloud cover). For sea ice covered surfaces, increased mixing ($\mu = 5$) leads to reduced total cloud cover during winter and spring, while in summer

20   it leads to an increase in cloud cover compared to base run ($\mu = 1$). For decreased mixing ($\mu = 0.2$), exactly the opposite is simulated, with more clouds in winter and few clouds during summer compared to the base run. Even if the cloud cover bias is reduced in the runs with increased mixing, the modeled cloud cover is still higher compared to CALISPO during winter, while only minor changes in the cloud cover bias are found for summer. Total cloud cover behaves similarly for increased/decreased mixing whenever a grid box is snow covered (no information is available during summer as no grid box is snow-covered), and

25   cloud cover is also overestimated for all runs during winter compared to CALIPSO. In general, increased mixing is expected to increase the moisture fluxes from the surface into the atmosphere and therefore to increase the moisture availability in the lowest levels of the atmosphere. While this assumption is valid for most parts of the globe, heat fluxes in the Arctic can reverse during winter so that fluxes of sensible and latent heat from the lowest layers of the atmosphere are directed towards the surface. This is due to the often observed low-level temperature inversion that also leads to qualitatively similar moisture profiles

30   as saturation water vapor content is a function of temperature. In case of such a moisture inversion, increased mixing increases the latent heat fluxes from the atmosphere onto the surface, and this process is a sink for atmospheric moisture. In case of a temperature inversion, stronger mixing causes surface temperatures to increase, but the effect of this temperature increase on cloud cover is twofold. On the one hand, warmer surface temperatures make the atmospheric stratification less stable, which further increases mixing and consequently leads to stronger removal of atmospheric moisture by latent heat fluxes as long as the moisture inversion is still present. On the other hand, a warmer surface increases the moisture content. Consequently, the vertical moisture gradient is weakened, also resulting in weaker moisture fluxes from the atmosphere onto the surface according to Equation 1. Altogether, the increased moisture removal seems to dominate over the decrease in vertical moisture gradient, as cloud cover is reduced due to stronger mixing. Despite the potential to improve cloud cover by stronger surface mixing over

5 snow and ice covered surfaces, it is questionable whether one can physically justify to further increase mixing as most climate models already mix too strongly in stable boundary layers (Holtslag et al., 2013). We will further elaborate on that in the next section.

Besides the rather straightforward influence of surface properties on surface mixing strength, misrepresented cloud microphysical processes also affect cloud cover in the Arctic. As we have shown in the previous section, it is mainly the low-level, liquid

10 containing clouds that cause this observed cloud cover bias. Low-level clouds in the Arctic are typically mixed-phase clouds, so the overestimation of liquid clouds can be related to a misrepresentation of microphysical processes that act in this temperature regime, i.e., heterogeneous freezing of cloud liquid into ice or the production of cloud ice at the expense of cloud liquid water, also known as the Wegener-Bergeron-Findeisen process. In this study, we will focus primarily on the WBF process as it is an effective way of turning liquid into ice clouds by making the depositional growth of ice crystals more efficient. Depositional

15 growth of cloud ice takes place, according to the ECHAM6 parameterizations, if one of the following conditions is met:

1. $T < -35°\,\mathrm{C}$

2. $T < 0°\,\mathrm{C}$ and $x_i > \gamma_{\mathrm{thr}}$ (where x_i is the in-cloud ice water mass mixing ratio)

The second conditions can be seen as a simple parametrization of the WBF process, as it allows condensation of liquid water to take place for temperatures below $0°\,\mathrm{C}$ if the ice water mixing ratio within the cloud is below a certain value. Setting an

20 in-cloud ice water mixing ratio threshold is a reasonable condition for the onset of the WBF process within a cloud. Only after a sufficiently large number of crystals is formed by freezing, depositional growth of ice crystals will efficiently deplete any excess water vapor and supersaturation with respect to ice will relax back to unity (Kärcher and Lohmann, 2003). In the standard setup, γ_{thr} is set to $5 \cdot 10^{-6}$ $\mathrm{kg\,m^{-3}}$, but this tuning parameter is resolution-dependent and can vary by an order of magnitude between the different horizontal resolutions of ECHAM6. We will evaluate how a reduction affects the total amount

25 and the partitioning between liquid and ice clouds in the model. Lower values of γ_{thr} increase the effectiveness of the WBF process, leading to less cloud water but more cloud ice to be present. As almost all precipitation in the Arctic is formed via the ice phase, a decrease of γ_{thr} is expected to eventually lead to a decrease in cloud cover as cloud condensate should be more efficiently removed via precipitation. As can be seen from Figure 5, decreasing γ_{thr} in fact leads to a reduction in low-level liquid-phased clouds winter, but the positive bias in total cloud cover remains more or less unchanged. This is striking, as one

30 would expect cloud cover to decrease due the stronger removal of cloud condensate by precipitation.

A possible explanation why changing the strength of the WBF process does not result in a significant change in cloud cover is the way saturation water vapor pressure is calculated in the cloud cover scheme. For temperatures below $0°\,\mathrm{C}$, the saturation water vapor pressure in ECHAM6 can either be calculated with respect to water or ice. As saturation water vapor pressure over ice decreases faster with decreasing temperature compared to the saturation water vapor pressure over water, relative humidity with respect to ice will be larger compared to relative humidity with respect to water at the same water vapor pressure at sub-zero temperatures. For the decision with respect to which phase state the saturation water vapor is calculated, ECHAM6 uses the same conditions as for the WBF process, so if depositional (condensational) growth of ice crystals (cloud droplets) takes place, saturation water vapor pressure is calculated with respect to ice (water). As cloud cover is diagnosed as a function

5 of grid-mean relative humidity (Sundqvist et al., 1989), the choice with respect to which phase state the saturation water vapor pressure is calculated has a significant effect on fractional cloud cover. For the same water vapor pressure, relative humidity and therefore cloud cover will be much higher if cloud ice content exceeds γ_{thr}. This explains why enhancing the efficiency of the WBF process by choosing lower values for γ_{thr} has only a minor effect on cloud cover. As one decreases γ_{thr}, saturation water vapor pressure is more frequently calculated with respect to ice, which allows clouds to form at lower water vapor contents.

10 Furthermore, as an existing liquid cloud starts glaciating, in this parameterization the cloud cover will increase instantaneously once the ice content exceeds the threshold. As the Sundqvist cloud cover scheme is not able to handle supersaturation with respect to ice, a grid box is also often completely cloud covered at sufficiently low temperatures (Lohmann et al., 2008; Bock and Burkhardt, 2016).

To avoid this sudden increase in cloud cover as soon as the ice water content becomes greater than γ_{thr}, we modified the cal-

15 culation of the saturation water vapor pressures in the cloud cover scheme by using a weighted average between the saturation water vapor pressures over liquid water, e_l, and ice, e_i:

$$e = e_l(1 - f_i) + e_i f_i. \tag{4}$$

f_i is a weighting factor where $f_i = 0$ for a water cloud, $f_i = 1$ for an ice cloud and $0 < f_i < 1$ for a mixed-phase cloud (Korolev and Isaac, 2006). One commonly used approach to determine f_i is to define it as a temperature-dependent function that aims

20 to resemble the partitioning between cloud water and cloud ice with decreasing temperatures. We use a linear function that interpolates between the melting point $T_{\text{ice1}} = 0°\,\text{C}$ and the homogeneous freezing threshold $T_{\text{ice2}} = -35°\,\text{C}$ and define f_i as follows:

$$f_i = 1 - \frac{T - T_{\text{ice2}}}{T_{\text{ice1}} - T_{\text{ice2}}}. \tag{5}$$

f_i is set to 1 for temperatures lower than $-35°\,\text{C}$, while for $T > 0°\,\text{C}$, f_i is fixed to 0. In case the cloud ice content is less

25 than γ_{thr}, we also set f_i to 0. This condition is used to delay cloud formation as long as there is not enough cloud ice for the WBF process to efficiently produce cloud ice and the phase of the clouds is predominantly liquid. Compared to the previous way of defining the saturation water vapor, this new approach introduces supersaturation with respect to ice of up to 10% for clouds in the temperature regime of mixed-phase clouds. In Figure 6, we compare the effects of this new saturation water vapor pressure calculation (NEW) to the standard calculation for low-level cloud cover (BASE) in DJF for different settings of γ_{thr}.

30 For the standard setting of γ_{thr} the NEW implementation has its largest impact in the storm tracks of the Atlantic and the Pacific ocean, where cloud cover is reduced quite significantly, while for continental regions, almost no difference to the BASE run is simulated. In contrast to the BASE runs, decreasing γ_{thr} in the NEW runs reduces the cloud cover in almost all continental regions north of 60°N. Some regions within Siberia and the ice covered Arctic ocean show only a small reduction in cloud cover and are comparable to the BASE runs. As temperatures in those regions easily can reach values below the homogeneous

5 freezing threshold, only minor changes can be expected, as for both implementations saturation water vapor pressure with respect to ice is used to calculate relative humidity. The decrease in γ_{thr} also further strengthens the reduction of cloud cover in the storm-track regions. Possibly, further parameter tuning of cloud microphysical processes (e.g., reduced condensate removal

by precipitation) can improve this newly introduced cloud cover bias in the oceanic regions, but this is not the subject of this study.

5 Discussion

In the previous sections, we showed that ECHAM6 overestimates low-level cloud cover over snow- and ice-covered surfaces during wintertime. While the partitioning of liquid and ice clouds can be improved by a more effective WBF process, the overall positive cloud cover bias could not be reduced by that measure alone. We showed that this positive cloud cover bias can be improved by either a more effective mixing at the surface or by an alternative approach of calculating the saturation water vapor pressure in the cloud cover scheme.

As we have already stated in the previous section, further increasing mixing over snow and ice covered regions is not desirable as climate models in general mix too strongly under these conditions. That this is also the case for ECHAM6 can be confirmed by two different aspects within the parametrization of the surface mixing in ECHAM6. In the following, we only discuss mixing over sea ice, but the conclusions are to some extent also valid for snow covered surfaces. From Equation 2, we see that the bulk exchange coefficient that governs the strength of mixing in ECHAM6 is calculated as the product of the neutral limit transfer coefficient $C_{N,\psi}$ and a (surface-layer) stability function f_ψ. The roughness length for both momentum and scalars is set to $z_{0,h/m} = 10^{-3}$ m over sea ice, which is rather large compared to observations. Citing several observational studies, Gryanik and Lüpkes (2018) stated that roughness length for momentum over ice covered surface can have values ranging between $z_{0,m} = 7 \cdot 10^{-6}$ m and $z_{0,m} = 5 \cdot 10^{-2}$ m with an average value of $z_{0,m} = 3.3 \cdot 10^{-4}$ m (Castellani et al., 2014), but surface roughness can locally be enhanced way beyond the values given by Gryanik and Lüpkes (2018), e.g. in the marginal sea ice zones or at large sea ice ridges in the central Arctic or near Greenland (Lüpkes et al., 2012). The average value is already an order of magnitude lower then the roughness length used in ECHAM6, so neutral limit transfer coefficients are also larger than the observations suggest. The same is true for the stability function f_ψ over sea ice in stable regimes. Gryanik and Lüpkes (2018) compared the stability functions used in ECHAM6 (Louis, 1979) to an alternative formulation of those functions that were derived from the SHEBA dataset (Grachev et al., 2007) and should be better suited for stable stratification over sea ice. While for weaker stability, the presently used stability functions are in agreement with this new formulation, they are considerably larger for stronger stability. As both the presently used roughness length over ice covered surface and the stability functions applied in ECHAM6 already produce stronger mixing than observed, we think that increasing mixing efficiency even further might not be a reasonable measure to reduce cloud cover.

As climate models in general struggle to represent microphysical processes correctly, attributing the positive bias in cloud cover to misrepresented microphysical processes seems not to be far-fetched. By exploring the sensitivity of cloud cover to changes in the effectiveness of the WBF process, we showed that the way microphysical processes act is not straightforward, as one might expect a higher removal of atmospheric moisture for a higher cloud ice content that should eventually decrease cloud cover. Nevertheless, increasing the effectivness of the WBF processes helped to reduce the liquid cloud amount at the expense of an increased ice cloud amount. Klaus et al. (2012) found a similar increase for wintertime cloud amount

for increasing and decreasing commonly used microphysical tuning parameters for this scheme in a single column setup of the regional Arctic climate model HIRHAM5 (similar, but older version of the ECHAM6 physical parametrizations). For all their sensitivity studies, cloud condensate always increased despite larger precipitation rates, so it seems that other processes
10 overcompensated this enhanced removal of atmospheric moisture. As it seems impossible to reduce cloud cover in ECHAM6 through microphysics alone, we switched to a different approach for calculating saturation water vapor pressure in the cloud cover scheme. By using a temperature-dependent linear function that interpolates between saturation with respect to water and saturation with respect to ice, we were able to reduce cloud cover in the temperature range of typical mixed-phase clouds. Previously, the decision with respect to which phase the saturation water vapor pressure is calculated was primarily based on a
15 cloud ice threshold to be consistent with parametrization of the WBF within the microphysical scheme. For the WBF process, such a threshold is an appropriate choice because as soon as a certain amount of cloud ice is present a cloud quickly glaciates (Kärcher and Lohmann, 2003), but when used in the cloud cover parameterization it might introduce spurious increases in cloud cover when prexisting liquid clouds start to glaciate. By using a new temperature dependent calculation of the saturation water vapor pressure, we allowed for a slight supersaturation with respect to ice in the cloud cover scheme so that relative
20 humidity was reduced when diagnosing cloud cover using the Sundqvist scheme. Allowing for supersaturation with respect to ice is crucial to accurately represent mixed-phase and ice clouds as supersaturation with respect to ice is frequently observed in clouds that contain ice (Heymsfield et al., 1998; Gierens et al., 2000; Spichtinger et al., 2003; Korolev and Isaac, 2006). That cloud cover is still positively biased in Arctic regions with very cold temperatures emphasizes the need for a cloud cover parametrization that is designed to handle supersaturation with respect to ice even at temperatures below the homogeneous
25 freezing threshold. First attempts to implement such a parametrization were made by Bock and Burkhardt (2016), who used ECHAM5-HAM that uses a more sophisticated two-moment microphysics scheme that explicitly allows ice supersaturation (Lohmann et al., 2008). Bock and Burkhardt (2016) primarily evaluated their new scheme for cirrus clouds, but it is to be expected that such an approach might also improve low-level cloud cover in the Arctic as those clouds often contain ice. Klaus et al. (2016) used a different approach to reduce Arctic cloud cover for their regional Arctic climate model HIRHAM5 (same
30 physical parametrizations as ECHAM6 but different dynamical core). Instead of using the diagnostic Sundqvist scheme with its uniform probability density function, they used the statistical Tompkins (2002) cloud cover scheme and modified the shape of the beta function that is used as the probability density function to diagnose cloud cover. By making the beta function negatively skewed, they were able to reduce the positive cloud cover bias in their model.

6   Conclusions

Correctly simulating the Arctic climate is a big challenge for climate models. Especially mixed-phased clouds pose a challenge for these models, as many of the processes acting in mixed-phase clouds are only poorly understood, which makes it even harder to develop parametrizations that can represent those processes at grid sizes of a typical climate model. A typical feature
5 that many models struggle to correctly simulate are the often observed two distinct atmospheric states in the Arctic: a radiatively clear state with small cloud cover or thin, ice containing clouds in combination with a strong surface-based inversion, and a

cloudy state with low-level, liquid or mixed-phase clouds and only weak longwave cooling at the surface, which results in a
weak and often elevated inversion (Stramler et al., 2011). Pithan et al. (2014) showed that a majority of current climate models
lack a realistic representation of the cloudy state, which they attribute to an inadequate mixed-phase cloud microphysics. Our

10 study shows that ECHAM6 is one of the few models that actually overestimates cloud cover in the Arctic. This overestimation
also becomes obvious in the intercomparison of the cloud radiative effect (CRE) of several models that participated in CMIP5.
Boeke and Taylor (2016) showed that the MPI-ESM-LR/MR earth system model which has ECHAM6 as its atmospheric
component, exceeds the multi-model ensemble mean net Arctic CRE ($16.86\,\mathrm{W\,m^{-2}}$) by roughly $10\,\mathrm{W\,m^{-2}}$ (MPI-ESM-LR:
$26.00\,\mathrm{W\,m^{-2}}$ /MPI-ESM-MR: $24.49\,\mathrm{W\,m^{-2}}$) but is in far better agreement with the CERES-EBAF net CRE of $24.22\,\mathrm{W\,m^{-2}}$.

15 Even if the net CRE is in agreement with CERES-EBAF, the shortwave CRE (more negative) and the longwave CRE (more
positive) do not match the observed values, which can be linked to the overestimated cloud cover in MPI-ESM-LR/MR.
Allowing for gentle supersaturation with respect to ice in the cloud cover scheme, we were able to reduce to observed bias in
ECHAM6 to a large extent. This emphasizes the need for a cloud cover parametrization that is explicitly designed to handle
supersaturation. We also explored the sensitivity of cloud cover to modified surface fluxes, and even if we were not able reduce

20 the cloud cover bias in ECHAM6 using reasonable parameter settings, decreasing the surface fluxes in other models might help
to improve the representation of the cloudy state in other climate models.

Author contributions. JK and JQ this conceived this study. JM and MS helped to set up COSP in ECHAM6 and helped in conducting the
model runs. MS further contributed by providing valuable expertise on the physical parametrizations of ECHAM6. All of the authors assisted
with the interpretation of the results. JK prepared the manuscript with contributions from all co-authors.

5   *Competing interests.* The authors declare that they have no conflict of interest.

Disclaimer. TEXT

Acknowledgements. This study was funded by the German Research Foundation (Deutsche Forschungsgemeinschaft, DFG) Collaborative
research centre SFB/TR 172 "ArctiC Amplification: Climate Relevant Atmospheric and SurfaCe Processes, and Feedback Mechanisms,
$(AC)^3$ " in sub-project D02. The ECHAM6 model is developed by the Max Planck Institute for Meteorology, Hamburg, and we thank the
10 colleagues for making the model available to the research community. Simulations were conducted at the German Climate Computing Centre
(Deutsches Klimarechenzentrum, DKRZ). We would like to thank NASA and CNES for operating the CALIPSO satellite, as well as the data
producers for the satellite data used in this study.

References

Barton, N. P., Klein, S. A., Boyle, J. S., and Zhang, Y. Y.: Arctic synoptic regimes: Comparing domain-wide Arctic cloud observations with CAM4 and CAM5 during similar dynamics, Journal of Geophysical Research Atmospheres, 117, https://doi.org/10.1029/2012JD017589, 2012.

Bock, L. and Burkhardt, U.: The temporal evolution of a long-lived contrail cirrus cluster: Simulations with a global climate model, Journal of Geophysical Research, 121, 3548–3565, https://doi.org/10.1002/2015JD024475, 2016.

Bodas-Salcedo, A., Webb, M. J., Bony, S., Chepfer, H., Dufresne, J. L., Klein, S. A., Zhang, Y., Marchand, R., Haynes, J. M., Pincus, R., and John, V. O.: COSP: Satellite simulation software for model assessment, Bulletin of the American Meteorological Society, 92, 1023–1043, https://doi.org/10.1175/2011BAMS2856.1, 2011.

Boeke, R. C. and Taylor, P. C.: Evaluation of the Arctic surface radiation budget in CMIP5 models, Journal of Geophysical Research: Atmospheres, 121, 8525–8548, https://doi.org/10.1002/2016JD025099, 2016.

Castellani, G., Lüpkes, C., Hendricks, S., and Gerdes, R.: Variability of Arctic sea-ice topography and its impact on the atmospheric surface drag, Journal of Geophysical Research: Oceans, 119, 6743–6762, https://doi.org/10.1002/2013JC009712, 2014.

Cesana, G. and Chepfer, H.: Evaluation of the cloud thermodynamic phase in a climate model using CALIPSO-GOCCP, Journal of Geophysical Research Atmospheres, 118, 7922–7937, https://doi.org/10.1002/jgrd.50376, 2013.

Chepfer, H., Bony, S., Winker, D., Chiriaco, M., Dufresne, J. L., and Sèze, G.: Use of CALIPSO lidar observations to evaluate the cloudiness simulated by a climate model, Geophysical Research Letters, 35, https://doi.org/10.1029/2008GL034207, 2008.

Chepfer, H., Bony, S., Winker, D., Cesana, G., Dufresne, J. L., Minnis, P., Stubenrauch, C. J., and Zeng, S.: The GCM-oriented CALIPSO cloud product (CALIPSO-GOCCP), Journal of Geophysical Research Atmospheres, 115, https://doi.org/10.1029/2009JD012251, 2010.

Dee, D. P., Uppala, S. M., Simmons, A. J., Berrisford, P., Poli, P., Kobayashi, S., Andrae, U., Balmaseda, M. A., Balsamo, G., Bauer, P., Bechtold, P., Beljaars, A. C. M., van de Berg, L., Bidlot, J., Bormann, N., Delsol, C., Dragani, R., Fuentes, M., Geer, A. J., Haimberger, L., Healy, S. B., Hersbach, H., Hólm, E. V., Isaksen, L., Kållberg, P., Köhler, M., Matricardi, M., McNally, A. P., Monge-Sanz, B. M., Morcrette, J.-J., Park, B.-K., Peubey, C., de Rosnay, P., Tavolato, C., Thépaut, J.-N., and Vitart, F.: The ERA-Interim reanalysis: configuration and performance of the data assimilation system, Quarterly Journal of the Royal Meteorological Society, 137, 553–597, https://doi.org/10.1002/qj.828, 2011.

English, J. M., Kay, J. E., Gettelman, A., Liu, X., Wang, Y., Zhang, Y., and Chepfer, H.: Contributions of clouds, surface albedos, and mixed-phase ice nucleation schemes to Arctic radiation biases in CAM5, Journal of Climate, 27, 5174–5197, https://doi.org/10.1175/JCLI-D-13-00608.1, 2014.

English, J. M., Gettelman, A., and Henderson, G. R.: Arctic radiative fluxes: Present-day biases and future projections in CMIP5 models, Journal of Climate, 28, 6019–6038, https://doi.org/10.1175/JCLI-D-14-00801.1, 2015.

Francis, J. A. and Vavrus, S. J.: Evidence linking Arctic Amplification to Extreme Weather, Geophysical Research Letters, 39, 1–6, https://doi.org/10.1029/2012GL051000, 2012.

Gierens, K., Schumann, U., Helten, M., Smit, H., and Wang, P.-H.: Ice-supersaturated regions and subvisible cirrus in the northern midlatitude upper troposphere, Journal of Geophysical Research: Atmospheres, 105, 22 743–22 753, https://doi.org/10.1029/2000JD900341, 2000.

Grachev, A. A., Andreas, E. L., Fairall, C. W., Guest, P. S., and Persson, P. O. G.: SHEBA flux–profile relationships in the stable atmospheric boundary layer, Boundary-Layer Meteorology, 124, 315–333, https://doi.org/10.1007/s10546-007-9177-6, 2007.

Gryanik, V. M. and Lüpkes, C.: An Efficient Non-iterative Bulk Parametrization of Surface Fluxes for Stable Atmospheric Conditions Over Polar Sea-Ice, Boundary-Layer Meteorology, 166, 301–325, https://doi.org/10.1007/s10546-017-0302-x, 2018.

15 Heymsfield, A. J., Miloshevich, L. M., Twohy, C., Sachse, G., and Oltmans, S.: Upper-tropospheric relative humidity observations and implications for cirrus ice nucleation, Geophysical Research Letters, 25, 1343–1346, https://doi.org/10.1029/98GL01089, 1998.

Holtslag, A. A. M., Svensson, G., Baas, P., Basu, S., Beare, B., Beljaars, A. C. M., Bosveld, F. C., Cuxart, J., Lindvall, J., Steeneveld, G. J., Tjernström, M., and Van De Wiel, B. J. H.: Stable Atmospheric Boundary Layers and Diurnal Cycles: Challenges for Weather and Climate Models, Bulletin of the American Meteorological Society, 94, 1691–1706, https://doi.org/10.1175/BAMS-D-11-00187.1, 2013.

20 Intrieri, J. M.: An annual cycle of Arctic surface cloud forcing at SHEBA, Journal of Geophysical Research, 107, 8039, https://doi.org/10.1029/2000JC000439, 2002.

Kärcher, B. and Lohmann, U.: A parameterization of cirrus cloud formation: Heterogeneous freezing, Journal of Geophysical Research, 108, 4402, https://doi.org/10.1029/2002JD003220, 2003.

Karlsson, J. and Svensson, G.: Consequences of poor representation of Arctic sea-ice albedo and cloud-radiation interactions in the CMIP5 25 model ensemble, Geophysical Research Letters, 40, 4374–4379, https://doi.org/10.1002/grl.50768, 2013.

Karlsson, K.-G. and Dybbroe, A.: Evaluation of Arctic cloud products from the EUMETSAT Climate Monitoring Satellite Application Facility based on CALIPSO-CALIOP observations, Atmospheric Chemistry and Physics, 10, 1789–1807, https://doi.org/10.5194/acp-10-1789-2010, 2010.

Kay, J. E. and L'Ecuyer, T.: Observational constraints on Arctic Ocean clouds and radiative fluxes during the early 21st century, Journal of 30 Geophysical Research Atmospheres, 118, 7219–7236, https://doi.org/10.1002/jgrd.50489, 2013.

Kay, J. E., Bourdages, L., Miller, N. B., Morrison, A., Yettella, V., Chepfer, H., and Eaton, B.: Evaluating and improving cloud phase in the Community Atmosphere Model version 5 using spaceborne lidar observations, Journal of Geophysical Research: Atmospheres, 121, 4162–4176, https://doi.org/10.1002/2015JD024699, 2016.

Klaus, D., Dorn, W., Dethloff, K., Rinke, A., and Mielke, M.: Evaluation of Two Cloud Parameterizations and Their Possible Adaptation to 35 Arctic Climate Conditions, Atmosphere, 3, 419–450, https://doi.org/10.3390/atmos3030419, 2012.

Klaus, D., Dethloff, K., Dorn, W., Rinke, A., and Wu, D. L.: New insight of Arctic cloud parameterization from regional climate model simulations, satellite-based, and drifting station data, Geophysical Research Letters, 43, 5450–5459, https://doi.org/10.1002/2015GL067530, 2016.

Korolev, A. and Isaac, G. A.: Relative Humidity in Liquid, Mixed-Phase, and Ice Clouds, Journal of the Atmospheric Sciences, 63, 2865–2880, https://doi.org/10.1175/JAS3784.1, 2006.

5 Liu, Y., Ackerman, S. A., Maddux, B. C., Key, J. R., and Frey, R. A.: Errors in cloud detection over the arctic using a satellite imager and implications for observing feedback mechanisms, Journal of Climate, 23, 1894–1907, https://doi.org/10.1175/2009JCLI3386.1, 2010.

Liu, Y., Key, J. R., Liu, Z., Wang, X., and Vavrus, S. J.: A cloudier Arctic expected with diminishing sea ice, Geophysical Research Letters, 39, https://doi.org/10.1029/2012GL051251, 2012.

Lohmann, U., Spichtinger, P., Jess, S., Peter, T., and Smit, H.: Cirrus cloud formation and ice supersaturated regions in a global climate 10 model, Environmental Research Letters, 3, 045 022, https://doi.org/10.1088/1748-9326/3/4/045022, 2008.

Louis, J.-F.: A parametric model of vertical eddy fluxes in the atmosphere, Boundary-Layer Meteorology, 17, 187–202, https://doi.org/10.1007/BF00117978, 1979.

Lüpkes, C., Gryanik, V. M., Hartmann, J., and Andreas, E. L.: A parametrization, based on sea ice morphology, of the neutral atmospheric drag coefficients for weather prediction and climate models, Journal of Geophysical Research Atmospheres, 117, 1–18, https://doi.org/10.1029/2012JD017630, 2012.

Morrison, H., de Boer, G., Feingold, G., Harrington, J., Shupe, M. D., and Sulia, K.: Resilience of persistent Arctic mixed-phase clouds, Nature Geoscience, 5, 11–17, https://doi.org/10.1038/ngeo1332, 2011.

Nam, C. C. W. and Quaas, J.: Evaluation of clouds and precipitation in the ECHAM5 general circulation model using CALIPSO and cloudsat satellite data, Journal of Climate, 25, 4975–4992, https://doi.org/10.1175/JCLI-D-11-00347.1, 2012.

Nam, C. C. W., Quaas, J., Neggers, R., Siegenthaler-Le Drian, C., and Isotta, F.: Evaluation of boundary layer cloud parameterizations in the ECHAM5 general circulation model using CALIPSO and CloudSat satellite data, Journal of Advances in Modeling Earth Systems, 6, 300–314, https://doi.org/10.1002/2013MS000277, 2014.

Pithan, F., Medeiros, B., and Mauritsen, T.: Mixed-phase clouds cause climate model biases in Arctic wintertime temperature inversions, Climate Dynamics, 43, 289–303, https://doi.org/10.1007/s00382-013-1964-9, 2014.

Screen, J. A. and Simmonds, I.: The central role of diminishing sea ice in recent Arctic temperature amplification., Nature, 464, 1334–1337, https://doi.org/10.1038/nature09051, 2010.

Serreze, M. C. and Barry, R. G.: Processes and impacts of Arctic amplification: A research synthesis, Global and Planetary Change, 77, 85–96, https://doi.org/10.1016/j.gloplacha.2011.03.004, 2011.

Shupe, M. D. and Intrieri, J. M.: Cloud radiative forcing of the Arctic surface: The influence of cloud properties, surface albedo, and solar zenith angle, Journal of Climate, 17, 616–628, https://doi.org/10.1175/1520-0442(2004)017<0616:CRFOTA>2.0.CO;2, 2004.

Spichtinger, P., Gierens, K., and Read, W.: The global distribution of ice-supersaturated regions as seen by the Microwave Limb Sounder, Quarterly Journal of the Royal Meteorological Society, 129, 3391–3410, https://doi.org/10.1256/qj.02.141, 2003.

Stephens, G. L., Vane, D. G., Boain, R. J., Mace, G. G., Sassen, K., Wang, Z., Illingworth, A. J., O'Connor, E. J., Rossow, W. B., Durden, S. L., Miller, S. D., Austin, R. T., Benedetti, A., and Mitrescu, C.: The cloudsat mission and the A-Train: A new dimension of space-based observations of clouds and precipitation, Bulletin of the American Meteorological Society, 83, 1771—-1790+1742, https://doi.org/10.1175/BAMS-83-12-1771, 2002.

Stevens, B., Giorgetta, M., Esch, M., Mauritsen, T., Crueger, T., Rast, S., Salzmann, M., Schmidt, H., Bader, J., Block, K., Brokopf, R., Fast, I., Kinne, S., Kornblueh, L., Lohmann, U., Pincus, R., Reichler, T., and Roeckner, E.: Atmospheric component of the MPI-M earth system model: ECHAM6, Journal of Advances in Modeling Earth Systems, 5, 146–172, https://doi.org/10.1002/jame.20015, 2013.

Stramler, K., Del Genio, A. D., and Rossow, W. B.: Synoptically driven Arctic winter states, Journal of Climate, 24, 1747–1762, https://doi.org/10.1175/2010JCLI3817.1, 2011.

Sundqvist, H., Berge, E., and Kristjánsson, J. E.: Condensation and Cloud Parameterization Studies with a Mesoscale Numerical Weather Prediction Model, Monthly Weather Review, 117, 1641–1657, https://doi.org/10.1175/1520-0493(1989)117<1641:CACPSW>2.0.CO;2, 1989.

Tompkins, A. M.: A Prognostic Parameterization for the Subgrid-Scale Variability of Water Vapor and Clouds in Large-Scale Models and Its Use to Diagnose Cloud Cover, Journal of the Atmospheric Sciences, 59, 1917–1942, https://doi.org/10.1175/1520-0469(2002)059<1917:APPFTS>2.0.CO;2, 2002.

Webb, M. J., Andrews, T., Bodas-Salcedo, A., Bony, S., Bretherton, C. S., Chadwick, R., Chepfer, H., Douville, H., Good, P., Kay, J. E., Klein, S. A., Marchand, R., Medeiros, B., Siebesma, A. P., Skinner, C. B., Stevens, B., Tselioudis, G., Tsushima, Y., and Watanabe, M.:

490   The Cloud Feedback Model Intercomparison Project (CFMIP) contribution to CMIP6, Geoscientific Model Development, 10, 359–384,
         https://doi.org/10.5194/gmd-10-359-2017, 2017.

Winker, D. M., Pelon, J. R., and McCormick, M. P.: The CALIPSO mission: Spaceborne lidar for observation of aerosols and clouds, Proc.
         of SPIE vol. 4893, 4893, 1–11, https://doi.org/10.1117/12.466539, 2003.

Zygmuntowska, M., Mauritsen, T., Quaas, J., and Kaleschke, L.: Arctic clouds and surface radiation-a critical comparison of satellite re-
495   trievals and the ERA-interim reanalysis, Atmospheric Chemistry and Physics, 12, 6667–6677, https://doi.org/10.5194/acp-12-6667-2012,
         2012.
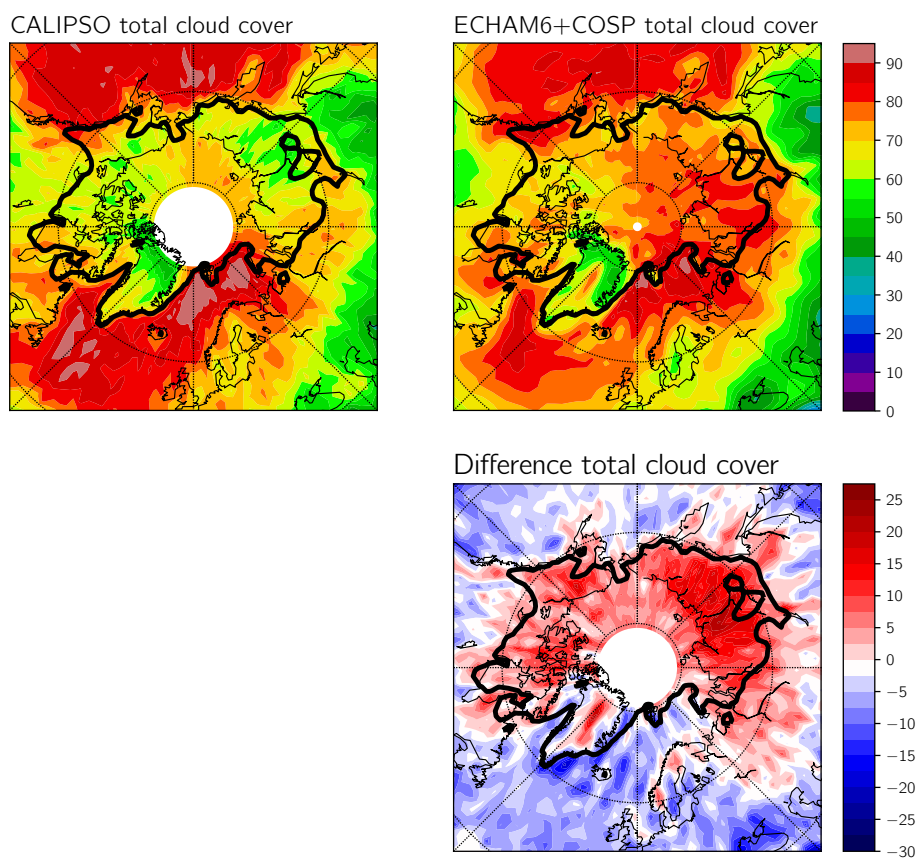
Figure 1. Top: Multi-year (2007-2011) mean total cloud cover as observed by CALIPSO and ECHAM6 + COSP. Bottom: Difference between the model and CALIPSO total cloud cover. Black line indicates regions with sea-ice cover greater then 50% or snow cover greater than 2 cm.
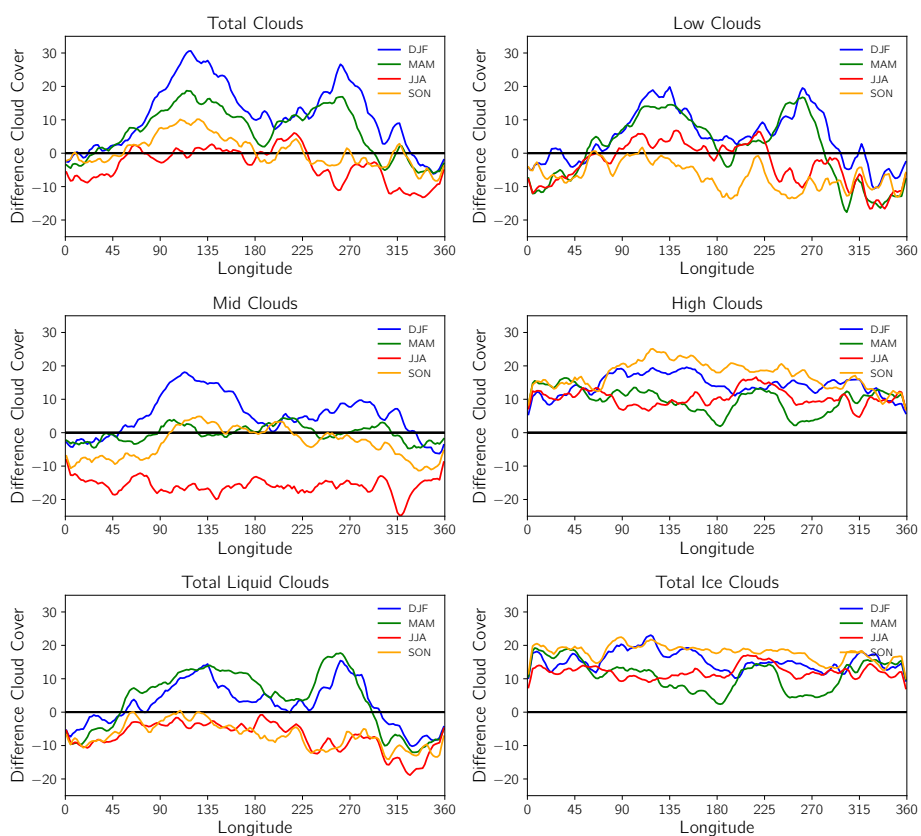
Figure 2. Meridional mean (60°N to 82°N) difference in cloud cover (model - satellite) vebetween ECHAM6 + COSP and CALIPSO for total, low, mid and high clouds as well as difference in total liquid and total ice cloud cover.
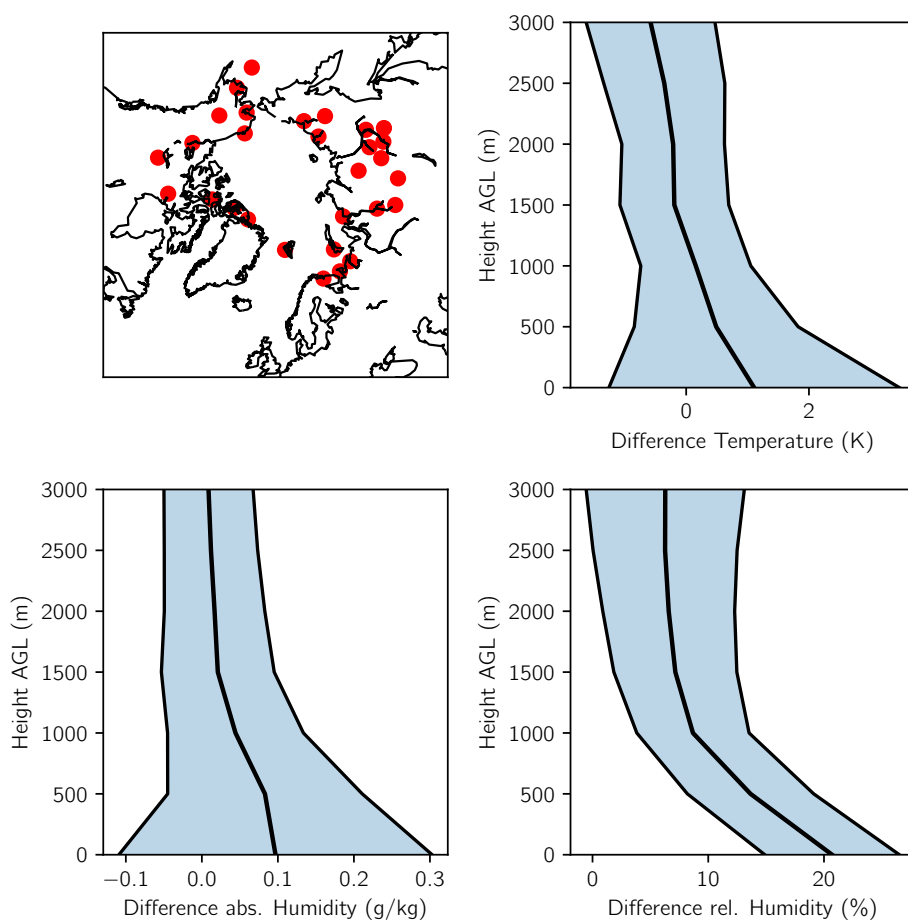
Figure 3. Vertical profiles of temperature, absolute humidity and relative humidity differences between ECHAM6 and several radiosonde launch location north of 60°N (as indicated by the red dots) averaged from 2007 to 2010. The vertical coordinate is height above ground level (AGL). Light blue shadings indicate one standard deviation.
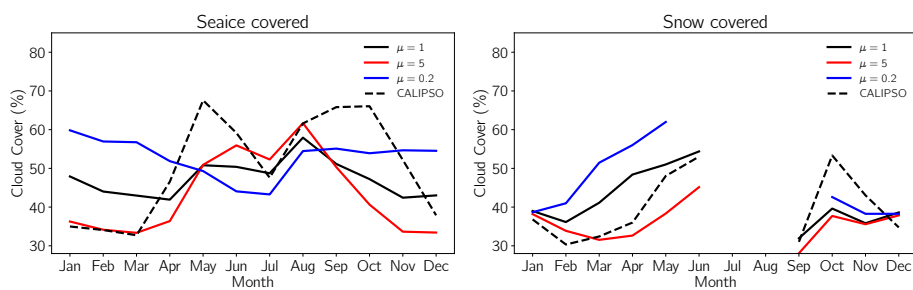
Figure 4. Low-level cloud cover over sea ice (left) and snow (right) covered surface for different strenght of near-surface mixing. For CALISPO cloud cover, ice/snow cover is used from base setup.
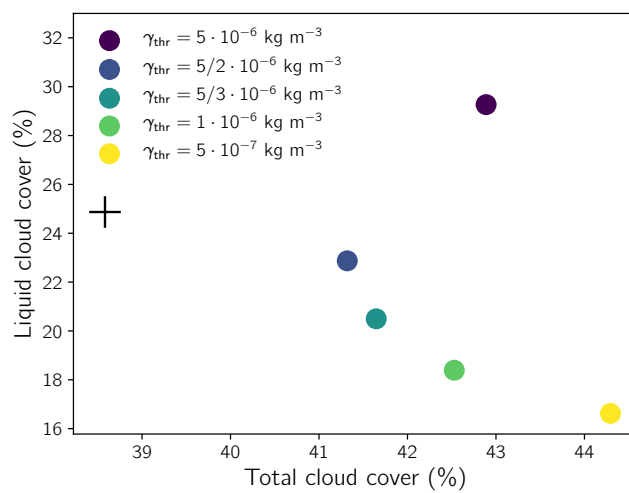
Figure 5. DJF low level liquid cloud cover compared to low level total cloud cover for different values of γ_{thr} (area-averged between $60°$N to $82°$N). The black cross are the values observed from CALIPSO.
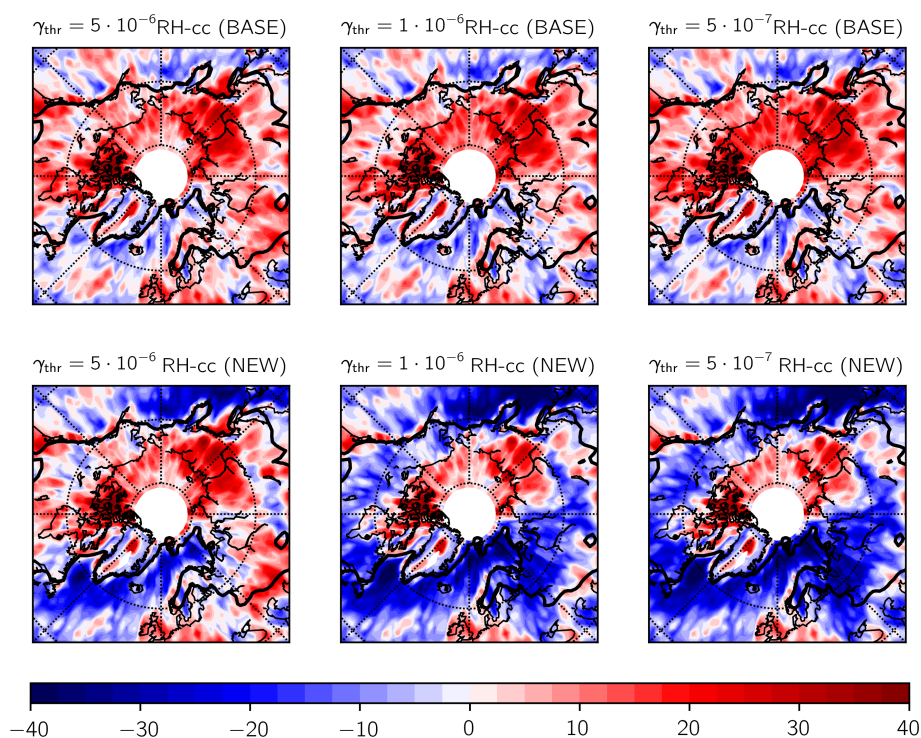
Figure 6. DJF low level cloud cover difference to CALIPSO for the BASE (top row) and NEW (bottom row) relative humidity calculation in the cloud cover scheme for different values of γ_{thr}.